ACS OMEGA

Open Access

This article is licensed under CC-BY 4.0

http://pubs.acs.org/journal/acsodf

Article

Evidence of High Fluorine Ion Conductivity in SrF_2-Rich SrF_2–TiO_2-Based Compounds

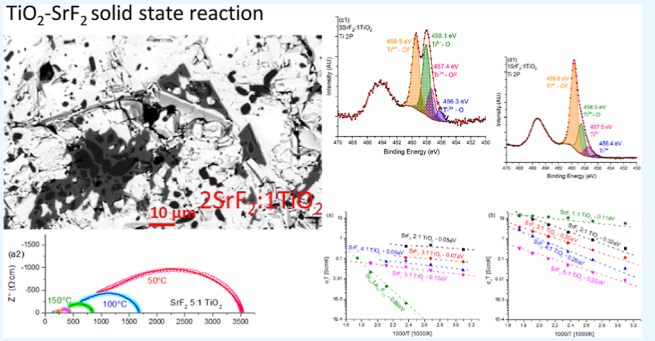
Yatir Sadia,* Gwilherm Kerherve, and Stephen J. Skinner

Cite This: *ACS Omega* 2025, 10, 19214–19223

Read Online

ACCESS | Metrics & More | Article Recommendations | Supporting Information

ABSTRACT: Materials based on Sr–Ti–O have shown remarkable properties and have been used in a wide diversity of applications. However, very little investigation has gone into the Sr–Ti–O–F system, mainly due to the very high stability of its constituents such as SrF_2 and TiO_2. In this work, solid-state reactions under reducing atmospheres on SrF_2 and TiO_2 showed highly interesting properties for the system, including high mixed electronic and ionic conductivity. XPS data further illuminate the results with the Ti 2p peaks shifting to higher binding energy due to fluorine interaction, possibly hinting at the formation of a TiO_xF_y phase. Testing using both ion blocking and electron blocking layers allowed the distinction between the ionic and electronic conductivity of the materials, showing very high ionic conductivity compared to most SrF_2-based compounds. Ionic conductivities of up to 1 mS cm^{-1} for $2SrF_2$:TiO_2 samples near room temperature were obtained. The ionic transport numbers were found to be 20–60% over the 50–300 °C temperature range. The apparent activation energy for ionic conduction was surprisingly low with E_a (ionic) = 0.05–0.10 eV for the different samples, whereas for electronic conductivity, E_a (electron) = 0.11–0.32 eV.



Downloaded via 146.179.166.101 on June 3, 2025 at 13:30:03 (UTC).
See https://pubs.acs.org/sharingguidelines for options on how to legitimately share published articles.

INTRODUCTION

Oxyfluoride materials are some of the most interesting materials for various applications. Oxyfluorides have been identified as interesting for battery applications for both fluoride-ion batteries[1−3] and lithium-ion batteries.[4−6] Oxyfluorides have been shown to conduct both oxygen[7,8] and fluorine[9,10] and have been identified as both superconductors[11,12] and materials for transparent electronics.[13,14] Some of the most interesting oxyfluorides come from systems where the composition is based on a perovskite such that $AB(O,F)_3$ is the representation of the material.[2,15,16] As such, $SrTi(O,F)_3$ might be enticing for research. Very little research has been done on $SrTiO_xF_y$ based materials, with most of it being achieved through fluorinating Sr_2TiO_4[17,19] and $Sr_3Ti_2O_7$.[18] This is done mainly using chemical fluorination using either NH_4F[17] or PVDF.[18] However, high-temperature synthesis from stable compounds such as TiO_2 and SrF_2 by reaction of the materials has not been thoroughly investigated.

SrF_2 is an insulating ceramic with a very wide band gap of 7.12 eV[20] and negligible ionic conductivity below 1000 °C.[21] Most applications for SrF_2 have been based on optical uses for UV and VUV spectroscopy.[22] With the correct doping, SrF_2 can be a good fluorine ion conductor. Doping SrF_2 with Ce,[23] Y and Na,[24] and Yb[25] achieved a maximum conductivity of 4.4 × 10^{-8} S·cm^{-1} at 227 °C with 10% Na, 0.4% Y, and 20.8% Yb and approximately 1.1 × 10^{-6} S·cm^{-1} for 23% Ce substitution at 127 °C.[23−25] The best dopant for SrF_2 seems to be La, with most conductivities reported as being around 8 × 10^{-2} S·cm^{-1} at 300 °C with 20% La[26] which was used as a reference material in this study. Conduction in SrF_2-based materials is almost purely ionic, with the electronic conductivity being 2–3 orders of magnitude lower. In SrF_2, the activation energy for conduction through fluorine vacancies is 0.4–0.7 eV,[26] while conduction through fluorine interstitials is closer to 0.75–0.95 eV.[26] Fluorine conductors can serve several applications, such as fluoride ion batteries, separation membranes for fluorine extraction, and fluorine detectors. While doped SrF_2 is a decent fluoride ion conductor, many fluoride ion conductors are much better conductors. The most studied are tysonite,[27−29] fluorite,[30−32] perovskite,[33−35] and amorphous glasses;[36−38] the most conductive samples are mainly based on $MSnF_4$-type materials.[39−43] By far, the best conductivity is shown by the $PbSnF_4$-based material in the β-structure phase.[40−43] The highest conductivities near a room temperature of 300 K are about 0.1 S·cm,[40−43] whereas the best perovskites such as $CsPb_{0.9}K_{0.1}F_{2.9}$ reach about 0.01 S·cm at 300 K.[33,34]

Received: March 13, 2025
Revised: April 5, 2025
Accepted: April 16, 2025
Published: April 28, 2025



© 2025 The Authors. Published by American Chemical Society

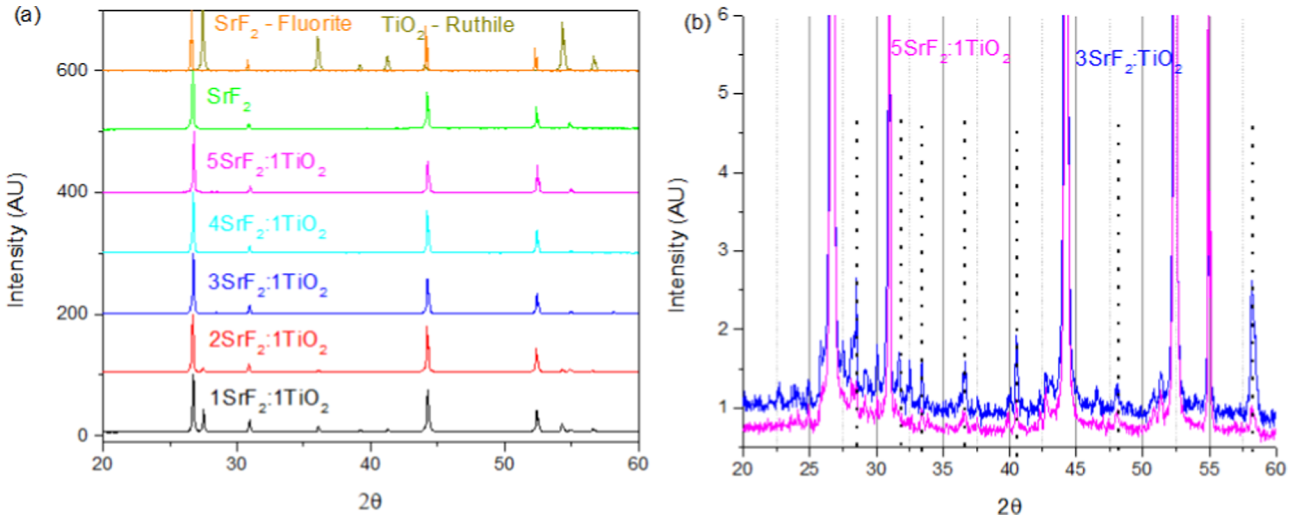


Figure 1. (a) XRD results for SrF_2:TiO_2 composites with the theoretical rutile and fluorite phases shown above (b), showing the small peaks of a secondary phase marked by dotted lines in $3SrF_2$:$1TiO_2$ and $5SrF_2$:$1TiO_2$; none of these peaks are above 3% intensity.

$TiO_{2-\delta}$ is an insulating ceramic with a band gap of 1.86 eV[44] and negligible electronic and ionic conductivity when $\delta = 0$.[45] However, when produced in a reducing environment, $TiO_{2-\delta}$ can show a wide range of electronic conductivities from slightly to highly conductive.[45−49] When reduced, oxygen vacancies in $TiO_{2-\delta}$ are compensated by excess electrons at first, leading to Ti^{3+} sites. Further increases in reduction introduce Ti^{3+} interstitials as well. In both regimes, however, the conduction is attributed to electrons, which are the major species. Oxygen ion conduction is very low for TiO_2-based materials, reaching only 10^{-4} S·cm^{-1} at 892 °C.[45] This figure is actually constant in different oxygen concentrations, as the compensation mechanisms in TiO_2 are based on electron and hole compensation, leading to electronic conductivity.

TiO_xF_y-type materials have been previously investigated, and they show high potential as photocatalysts,[50−53] as lithium-ion conductors for intercalation as anodes in lithium batteries,[54−57] and as electrochemical and super capacitors.[58,59] $TiOF_2$ is the stable phase discussed in all papers related to titanium oxyfluorides. $TiOF_2$ is hexagonal with a hexagonal to cubic transition near 50−60 °C.[60] It is conductive for both electrons and lithium ions and is a route to obtain different morphologies of anatase.[61,62]

$SrTiO_3$ is one of the semiconductors with the most diverse applications, finding uses in thermoelectric materials,[63−65] fuel cells,[66−68] biodiesel production,[69−71] and more. $SrTiO_3$-based materials, such as the layered perovskites of general composition ($Sr_{n+1}Ti_nO_{3n+1}$), show a semiconducting behavior with a band gap of 3.25 eV for $SrTiO_3$, 3.5 eV for Sr_2TiO_4, and 3.4 eV for $Sr_3Ti_2O_7$.[72] From the diverse properties of SrF_2, TiO_2, $TiOF_2$, and $SrTiO_3$, it is expected that any "$SrTiO_xF_y$"-type material should have interesting electrical properties and therefore direct reaction of SrF_2 and TiO_2 using a solid-state reaction should yield new materials with interesting functionality.

METHODOLOGY

Sample Preparation. SrF_2 (99.9%) and TiO_2 (99.8% TiO_2) powders purchased from Alfa Aesar were mixed in the ratios of 5:1, 4:1, 3:1, 2:1, and 1:1, respectively. Either 5 or 10 g of the mixtures were pressed in a 30 mm diameter graphite die using BN as a separator to produce 1.5 or 3 mm thick samples after grinding accordingly. The samples were heated at 13 °C/min to 800 °C and at 7.5 °C/min up to 1100 °C. The pressure was increased to a maximum of 28 MPa; at 1100 °C, the pressure was then slowly decreased to 2.8 MPa during 5 h of maintaining a temperature of 1100 °C. At this stage, the sample was cooled slowly to room temperature at 10 °C/min without pressure. The entire process was done in an argon UHP atmosphere with a custom-made graphite hot press from FCT GmbH (FCT, Germany). The samples were then ground to remove any traces of BN and graphite, and neither of these species was detected using energy-dispersive X-ray spectroscopy (EDS) or X-ray diffraction (XRD).

$La_{0.2}Sr_{0.8}F_{2.2}$ samples were produced by mixing SrF_2 powder with LaF_3 powder (99.9%) from Alfa Aesar in the relevant ratio and pressing them in the hot-press using the same conditions as the SrF_2−TiO_2 samples, while the layered samples were prepared by putting the mixed SrF_2−LaF_3 powders into the graphite die, then slightly pressing, then adding the SrF_2−TiO_2 samples and slightly pressing, and finally adding another layer of the $La_{0.2}Sr_{0.8}F_{2.2}$ and running the same process as mentioned above.

Characterization. XRD data were collected using a Panalytical Empyrean diffractometer with an X'Celerator detector with a Cu Kα source (λ = 1.5405 Å) operating at 40 kV and 30 mA, with analysis performed using the GSAS-II software package.[73] Scanning electron microscopy (SEM) was done with a JEOL-5600 operating at 15 keV using a backscattered electron detector (JEOL, Japan). Energy-dispersive X-ray spectroscopy was obtained using a Noran EDX-System (Thermo Fisher Scientific, USA).

X-ray photoelectron spectroscopy (XPS) was performed using a high-throughput X-ray photoelectron spectrometer (K-Alpha+, Thermo Fisher Scientific, US) with a monochromated Al Kα radiation source ($h\nu$ = 1486.6 eV) operating at a 2 × 10^{-9} mbar base pressure. The X-ray source used a 6 mA emission current and a 12 kV anode bias, giving an X-ray spot size of up to 400 μm^2. Survey and core-level spectra were obtained with pass energies of 200 and 35 eV, respectively. Spectra were processed by subtraction of a Shirley-type background, and peaks were fitted using a Gaussian−Lorentzian line shape.

https://doi.org/10.1021/acsomega.5c02253
ACS Omega 2025, 10, 19214−19223

Electrochemical Impedance Spectroscopy (EIS). EIS was performed by sputtering gold electrodes on both sides of 10 × 10 × 1 mm samples. Each sample was heated to 300 °C in 50 °C steps using a Carbolite tube furnace (Carbolite, UK) and a home-built rig, letting the samples equilibrate at each temperature for 1 h. The measurements were taken under the flow of Ar. The measurements were obtained over the frequency range of 1 MHz to 0.1 Hz using a Solartron 1260 Frequency Response Analyzer (Solartron, UK) with an AC amplitude of 100 mV. Pt wires and mesh on the rig were used for current collection. Data analysis was conducted using ZView4 software (Scribner, USA).

RESULTS

Microstructure. All samples showed a density of 4.1−4.2 g/cm^3, where 4.23 and 4.24 g/cm^3 are the theoretical densities of TiO_2 and SrF_2, respectively. All samples showed up to 3 distinct phases: SrF_2, $TiO_{2-\delta}$, and a small amount of an additional phase which contains mainly TiO_x, based on EDS analysis, but could not be identified by XRD as any known TiO_2 or Ti_xO_y phase. Predicted XRD peaks of the SrF_2 and TiO_2 phases are shown in Figure 1a. Examining a selected 2θ range, shown in Figure 1b, highlights small peaks at 28.51, 36.49, 40.55, and 58.12° 2θ shown here for 5-Sr:1-Ti and 3-Sr:1-Ti. However, no known phase is associated with these peaks, and their low intensity in the XRD pattern of under 3% for the highest intensity peak confirms this as a minor impurity phase. As shown in Figure 2d, SEM confirms that this unidentified phase is present in only small quantities with little to no connectivity, which is relevant for percolation. SEM backscattered micrographs are shown in Figure 2a−d for (a,c) 2-Sr:1-Ti and (b,d) 3-Sr:1-Ti. The white phase in Figure 2c is SrF_2, and the black phase is TiO_2, with the gray phase representing the unknown phase. In Figure 2d, only the white (SrF_2) and gray phases are shown as expected based on the XRD results. In Table 1, the ratio of the two main phases and the lattice parameters of the phases are shown. Little to no difference in the lattice parameters is seen. In places where the TiO_2 results were within the measurement error, they are marked in red, showing that they are present in the same amount as in the SrF_2-only sample, which contained no TiO_2. The density of all samples was found to be 4.2 g/cm^3 as measured by the Archimedes method, showing that samples had achieved a density of at least 98% of the theoretical value.

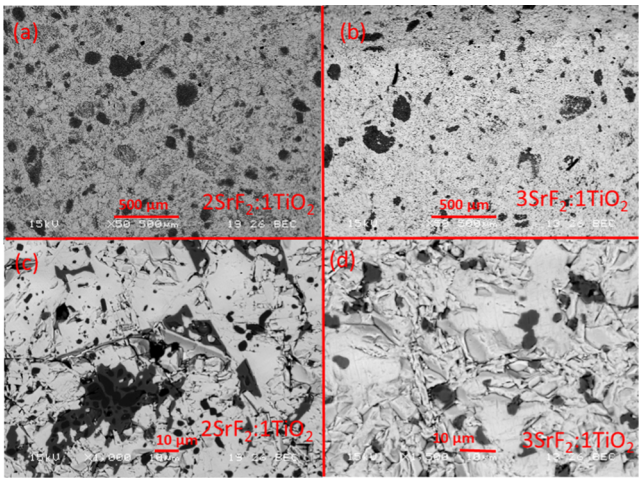


Figure 2. SEM micrographs obtained in backscattered electron mode. (a) and (b) showing $2SrF_2$:$1TiO_2$ showing 3 phases, TiO_2 in black embedded in an unknown gray phase and SrF_2 in white. (c) and (d) showing $3SrF_2$:$1TiO_2$ showing 3 phases, an unknown gray phase and SrF_2 in white. The unknown gray phase is about 10−15% SrF_2 and 85−90% TiO_2 based on EDS analysis.

X-ray Photoelectron Spectroscopy (XPS). XPS data were obtained for $1SrF_2$:$1TiO_2$ and $3SrF_2$:$1TiO_2$ initial ratios, along with the reference SrF_2 and TiO_2 samples produced in the same manner. Figure 3 shows the XPS results of the samples for (1) Ti 2p, (2) Sr 3d, (3) O 1s, and (4) F 1s. All samples have been corrected for the C−C C 1s feature at 284.8 eV. There are a number of initial key observations from the XPS analysis.

The highest energy Ti 2p feature is at 459.5 eV for the $3SrF_2$:$1TiO_2$ and $1SrF_2$:$1TiO_2$ samples. This is at a higher binding energy than expected from the reference TiO_2 sample with no SrF_2, which is at 458.6 eV. This agrees with literature data[60,76,77] for Ti^{4+} in some configuration of TiO_xF_y, identified as spectral features at 458.9−459.1 eV. This is understandable as Ti^{4+} from TiO_2 is observed at 458.6 eV and at 461.1 eV for TiF_4 as defined by Klimov et al.[78] Surprisingly, the TiO_2 sample shows only a negligible amount of Ti^{3+}, whereas the SrF_2:TiO_2 samples show Ti^{3+} in both the oxide state (Ti_2O_3) and the oxyfluoride (TiO_xF_y) state. This suggests that a higher number of vacancies were created in the Ti-rich phase. It also points to the Ti-rich phase in SEM as some unknown form of TiO_xF_y that does not fit a known XRD pattern. It is noteworthy that the ratio of oxide to oxyfluoride seems to be higher in the 1:1 ratio sample, whereas in the 3:1 sample, the ratio of oxide to oxyfluoride is about 1. The O 1s core level spectra show a shift toward higher binding energies going from 529.5 eV to about 531 eV, in agreement with previously reported oxyfluoride behavior.[76] Higher energy peaks associated with CO and OH were ignored as surface effects.

As for the Sr 3d peaks, SrF_2 showed a doublet at 133.5 and 135.3 eV, whereas the samples that contained TiO_2 as well showed another doublet at around 134.9 and 136.6 eV. A similar increase of the binding energy due to the presence of TiO_2 has been shown by Subash et al.,[79] and in epitaxial SrF_2,[80] Singh et al. have also attributed a peak at 136.5 eV to the SrF_2 reaction with oxygen in thin films, and fluorine doping in $SrTiO_3$ due to a reaction with HF has also been shown to increase the binding energy to 136.2 eV.[81] As for the fluorine peaks, only the $1SrF_2$:$1TiO_2$ sample shows a major peak movement; this makes sense as this sample shows the most pronounced TiO_xF_y in the Ti 2p spectrum and the most satellite peaks at 134.9/136.6 eV in the Sr 3d spectra.

From XPS, it is clear that (1) there is some formation of a TiO_xF_y type of phase which is more pronounced with greater TiO_2 content in the system. (2) The SrF_2 phase is shifted to higher energies for both F and Sr due to either loss of fluorine or exchange of fluorine with oxygen.

Electronic and Ionic Conductivities. Samples were coated with sputtered gold on both sides to provide F^- blocking layers.[82] The samples were measured at temperatures of up to 300 °C in steps of 50 °C.

The simplest circuit that fit most of the data was a shortened circuit, as seen in Figure 4. This circuit is based on the analysis by Huggins[83] with the electronic conductor marked by R_1 and an ionic conductor with blocking electrodes marked by R_2 and CPE_1, representing the resistance of the ionic conductor and the capacitance due to the blocking electrodes. An induction

https://doi.org/10.1021/acsomega.5c02253
ACS Omega 2025, 10, 19214−19223

Table 1. Fraction of TiO_2 and SrF_2 Obtained by Rietveld Refinement of XRD Data, with the Values for TiO_2 and SrF_2 Powders Put into the Sample before Hot Pressing by Weight Marked in Parentheses to Give a Reference for the Change[a]

Refinement parameters	1-Sr:1-Ti	2-Sr:1-Ti	3-Sr:1-Ti	4-Sr:1-Ti	5-Sr:1 -Ti	SrF_2	Theoretical
TiO_2% from refinement (before HP)	37.90% (38.87%)	11.20% (24.12%)	0% (17.49%)	0% (13.71%)	0% (11.28%)	0% (0%)	
SrF_2% from refinement (before HP)	62.10% (61.13%)	88.80% (75.88%)	100% (82.51%)	100% (86.29%)	100% (88.72%)	100% (100%)	
SrF_2 a [Å]=	5.8005(4)	5.7984(8)	5.7996(5)	5.7991(6)	5.7989(2)	5.8000(7)	5.8000 [74]
TiO_2 a [Å]=	4.6073(3)	4.6016(3)					4.5937 [75]
TiO_2 c [Å]=	2.9658(8)	2.9723(7)					2.9587 [75]

[a]Samples showing no TiO_2 after hot pressing (HP) are marked in red.

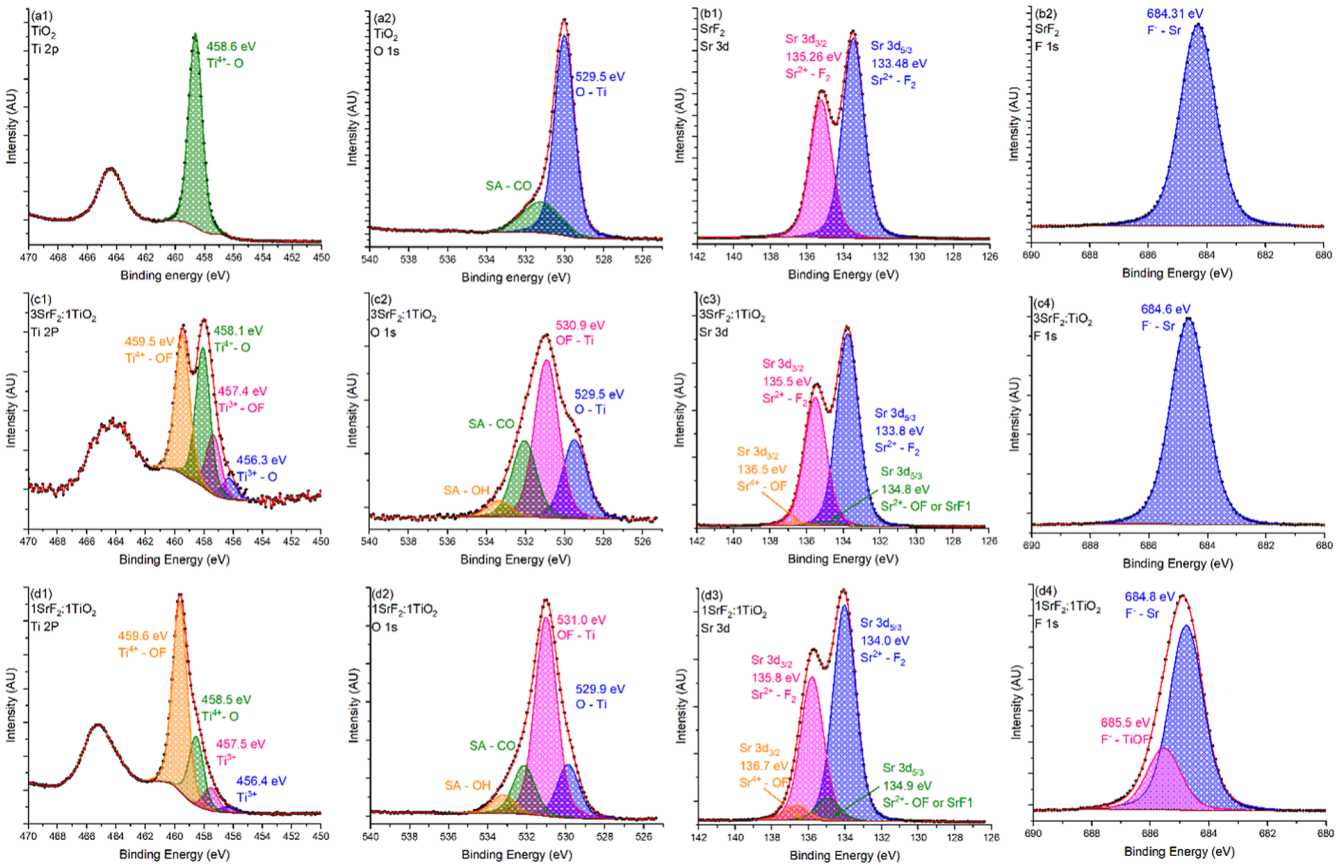


Figure 3. XPS of the (a) TiO_2 reference sample, (b) SrF_2, (c) $3SrF_2$:$1TiO_2$, and (d) $1SrF_2$:$1TiO_2$ with 1 Ti 2p, 2 O 1s, 3 Sr 3d, and 4 F 1s; here black is the original data, red is the fitting, and the rest of the colors are different peaks marked in the figure.

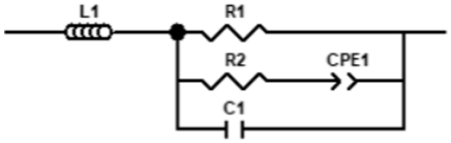


Figure 4. Short ion-conducting circuit with ion-blocking layers.

element was added to account for the wiring of the rig as suggested by Joncher.[84]

In Figure 5, the Nyquist plots of the EIS results for all samples are shown. These data are color-coded so that the results are in dashed lines with light red (50°), blue (100 °C), green (150 °C), magenta (200 °C), orange (250 °C), and purple (300 °C). The model results are in dotted dark red (50°), blue (100 °C), green (150 °C), magenta (200 °C), orange (250 °C), and purple (300 °C) markers. It can be seen that conductivity continued increasing with additional TiO_2 content. In addition, other than the 5:1 sample, all samples reach a temperature where the electronic conductivity far exceeds the ionic conductivity, resulting in complete electronic conductivity. The 4:1 sample turns mostly electronic between 200 and 250 °C, whereas for 3:1 and 2:1 that happens between 150 and 200 °C. With the 1:1 sample at all temperatures, the sample is mainly electronically conductive. Figure 5f shows the EIS of the SrF_2 sample to show that the ionic and electronic conductivity are not a simple result of combining electronically conductive $TiO_{2-\delta}$ and ionically conductive SrF_2 as SrF_2 is barely conductive in this temperature range. The results are very "shaky", and the model is not a perfect fit like in the other

https://doi.org/10.1021/acsomega.5c02253
ACS Omega 2025, 10, 19214−19223

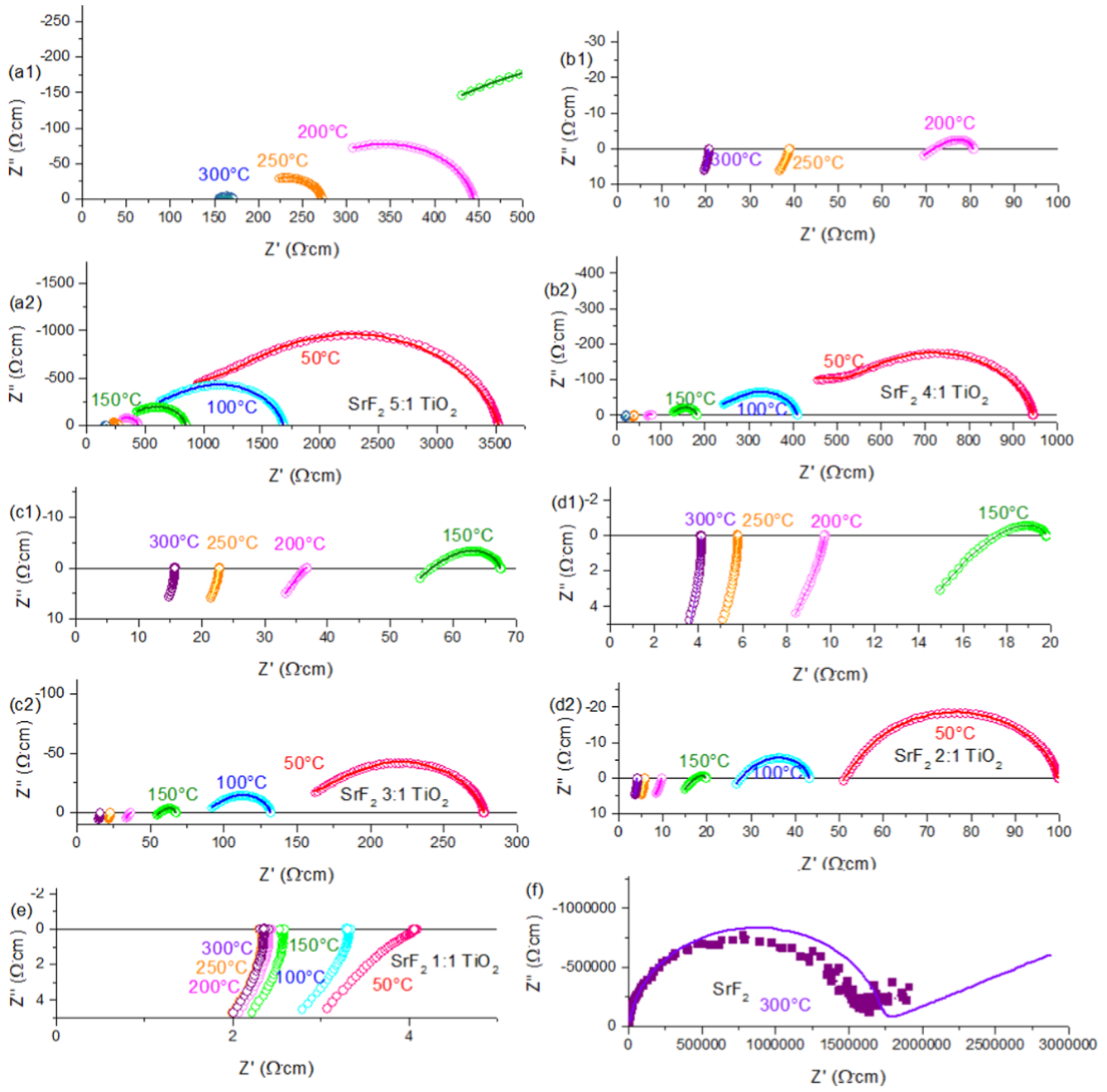


Figure 5. EIS spectra of all samples shown as Nyquist plots (a1−2) SrF_2 5:1 TiO_2 and (b1−2) SrF_2 4:1 TiO_2, (c1−2) SrF_2 3:1 TiO_2 and (d1−2) SrF_2 2:1 TiO_2, (e) SrF_2 1:1 TiO_2, and (f) SrF_2 only. Color coded so that the results are in dashes with light red (50°), blue (100 °C), green (150 °C), magenta (200 °C), orange (250 °C), and purple (300 °C). The model results are in dotted dark red (50°), blue (100 °C), green (150 °C), magenta (200 °C), orange (250 °C), and purple (300 °C).

circuits. This is due to the fact that pure SrF_2 is a very bad F-conductor even at 300 °C. This further proves that this is not the conduction source.

The short circuit is only relevant for transference numbers of above 10% ionic, meaning the ionic and electronic conductivities are within the same order of magnitude. In Table 2, the percentage of the ionic part of the transference number is shown. At any temperature where there were no results, the electronic conductivity was too high, and the ionic part was ignored in the analysis. The transference numbers are calculated to be between 64% and 10%.

To ensure that the ionic conductivity measured is not a different feature, electron-blocking layers of $La_{0.2}Sr_{0.8}F_{2.2}$ were used on both sides of the sample. Since $La_{0.2}Sr_{0.8}F_{2.2}$ blocks electrons and the gold layer blocks ions, the blocking layer

Table 2. Transference Numbers of the Ionic Species (F^-) vs the Overall Conductivity in All Samples

	transference number, τ_i %			
Temperature (°C)	2-Sr:1-Ti	3-Sr:1-Ti	4-Sr:1-Ti	5-Sr:1-Ti
50	46.1	37.1	44.2	63.7
100	33.8	26.6	35.7	55.0
150	14.9	14.8	24.8	44.3
200			10.5	30.7
250				24.3

https://doi.org/10.1021/acsomega.5c02253
ACS Omega 2025, 10, 19214−19223

analysis was performed using a regular non-shorted circuit seen in Figure 6, where R1 is the sum of the ionic resistance only of all 3 layers.

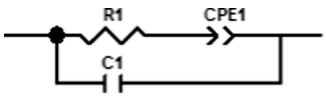


Figure 6. Blocking layer circuit.

Figure 7a shows the EIS data, while Figure 7b presents the conductivity results of $La_{0.2}Sr_{0.8}F_{2.2}$ (in black) and layered samples of $3SrF_2$:TiO_2 in red and SrF_2:TiO_2 in blue. It is clear from both Figure 7a,b that $3SrF_2$:TiO_2 is much more conductive than $La_{0.2}Sr_{0.8}F_{2.2}$, showing the same conductivity even with the extra layer of $3SrF_2$:TiO_2 in between the $La_{0.2}Sr_{0.8}F_{2.2}$ layers; this agrees with the results from the EIS data presented in Figure 4c and shown in magenta in Figure 7b. However, SrF_2:TiO_2 does not conduct F^- as well as seen from Figure 7a,b, showing that there is a 1 order of magnitude lower conductivity in SrF_2:TiO_2 than in $La_{0.2}Sr_{0.8}F_{2.2}$.

In Figure 8, we can see the electronic and ionic conductivities for all samples calculated based on the circuit shown in Figure 4. All samples show linear behavior for $\log(\sigma T)$ vs $1/T$, allowing an activation energy to be determined for all samples, which is shown in Figure 8b. In Figure 8a, the ionic conductivity is shown for all samples and temperatures at which the ionic conductivity was significant enough to separate from the electronic conductivity. In all samples, the activation energy was higher for the electronic conductivity than the ionic conductivity, preventing the measurement of ionic conductivity at high temperatures.

DISCUSSION

It can be seen that SrF_2−TiO_2-based materials show different properties than either TiO_2 or SrF_2. It seems that electronic conductivity arises from excess Ti^{3+} in the material from reduction of TiO_2, while ionic conductivity arises from a combination of a SrF_2 phase and a TiO_xF_y phase. The electronic activation energy is of the order of 0.2 eV for the samples that contain no $TiO_{2-\delta}$, about 0.32 eV for samples that contain small amounts (11%) of $TiO_{2-\delta}$, and 0.1 eV for the sample that contains $TiO_{2-\delta}$ above 30% as is usually needed for percolation.[85,86] This is an indication that the electronic conductivity is through the TiO_xF_y phase at low TiO_2 contents, whereas for high $TiO_{2-\delta}$ content, the conduction is through the $TiO_{2-\delta}$ phase. Another such explanation is that the conduction is increased at the interface between $TiO_{2-\delta}$ and SrF_2 due to space charge effects of F^- accumulation at the $TiO_{2-\delta}$ vacancies created by the reduction of $TiO_{2-\delta}$. This had been discussed in depth by Li et al.[87] This would explain why the highest conductivities are seen the closer we get to a 1:1 ratio of $TiO_{2-\delta}$ and SrF_2.

The activation energy of the ionic conductivity of $La_{0.2}Sr_{0.8}F_{2.2}$ was observed to be the same as the literature with within error at 0.69 eV.[88] The activation energies for the SrF_2:TiO_2-based materials were very low and much lower than those previously reported for the SrF_2-type materials. This is another indication that the conduction is mainly through a different phase, such as a TiO_xF_y phase. With the growth of the $TiO_{2-\delta}$ phase, a reduction in the ionic conductivity begins, as seen by the samples with LSF electron blocking layers. The activation energies of 0.05−0.10 eV are closer to those found in β-$PbSnF_4$ (0.2 eV)[39] and KSn_2F_5 (0.24 eV) at high temperatures[89] and 0.16 eV in the high-temperature phases in $RbPbF_3$. Even activation energies below 0.1 eV are seen on K-doped β-$PbSnF_4$[39] and in $CsPb_{0.9}K_{0.1}F_{2.9}$.[33,34] Such an extremely low activation energy is interesting, especially for room-temperature applications such as batteries, which require constant resistance across a wide range of temperatures. It is noteworthy that while the $TiO_{2-\delta}$ phase might have some amorphous qualities as it is unseen by XRD up to the 2:1 ratio sample, it is not common that amorphous materials have such a low activation energy[36−38] and does not seem to agree with the very low activation seen in these samples.

The fact that this material seems to be stable for a wide range of temperatures, is mechanically easier to prepare than most fluorite-based materials, and has low activation energies

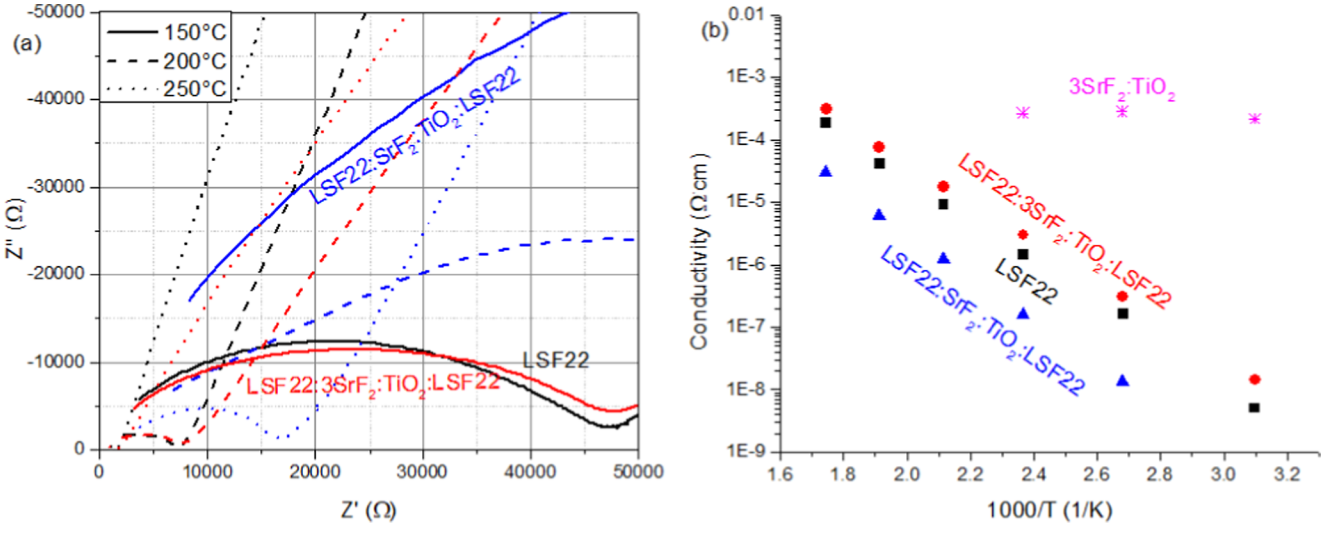


Figure 7. (a) EIS results from the samples with the blocking electrodes. $La_{0.2}Sr_{0.8}F_{2.2}$ in black, layered $La_{0.2}Sr_{0.8}F_{2.2}$: $3SrF_2$:TiO_2:$La_{0.2}Sr_{0.8}F_{2.2}$ in red, and $La_{0.2}Sr_{0.8}F_{2.2}$: $3SrF_2$:TiO_2:$La_{0.2}Sr_{0.8}F_{2.2}$ in blue. Data recorded at 150 °C shown as solid lines, 200 °C in dashed and 250 °C in dotted lines. (b) Summary of the ionic conductivity results as a function of temperature from the EIS data along with the values derived from the $3SrF_2$:TiO_2 sample added from previous results in magenta.

https://doi.org/10.1021/acsomega.5c02253
ACS Omega 2025, 10, 19214−19223

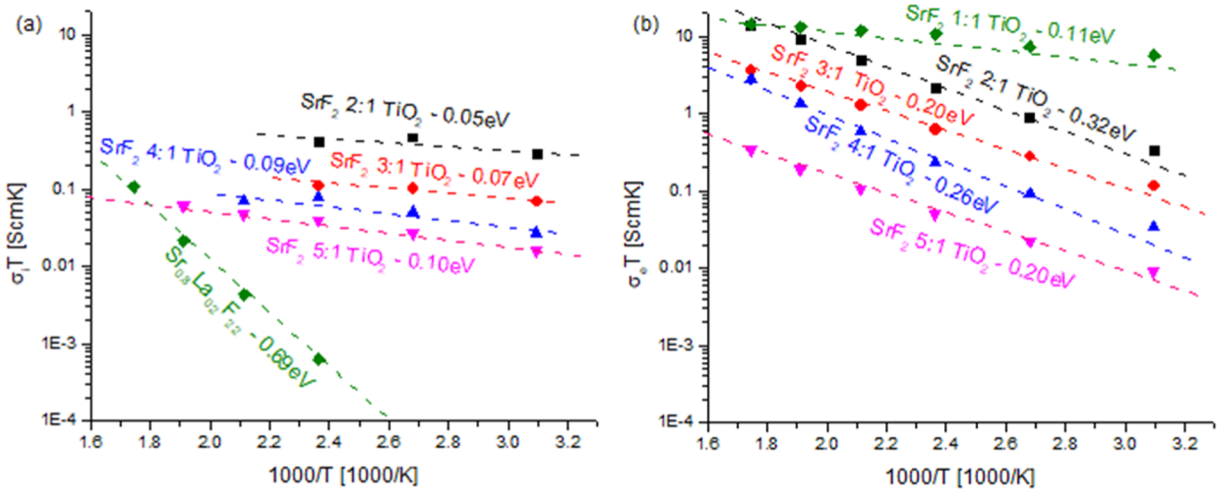


Figure 8. (a) σT_{ionic} vs reciprocal temperature showing linear behavior of the activation energy for the SrF_2:TiO_2 series. (b) $\sigma T_{electronic}$ vs reciprocal temperature showing linear activation energies for all samples.

for fluorine conduction near room temperature makes it very interesting for applications such as fluorine ion batteries. It is interesting to focus further in future studies on the ionic conduction mechanism to test if it could be decoupled from the electronic conductivity to allow for a wider range of applications.

CONCLUSIONS

SrF_2−TiO_2 composite materials have exhibited very interesting reactions, showing that some compositions form TiO_xF_y and also that there are changes in the behavior of the SrF_2 component. Materials based on this combination have shown very high conductivities for fluorine conduction due to fluorine moving from the SrF_2 component to the $TiO_{2-\delta}$ phase. Up to 25% TiO_2 can be added with little to no TiO_2 phase remaining, while maximum conductivity is observed with 33% TiO_2. Further increasing the TiO_2 content increases the electronic conductivity without increasing the ionic conductivity. Such materials can be interesting if control over the electronic/ionic conductivity ratio can be obtained by further studies.

ASSOCIATED CONTENT

Supporting Information

The Supporting Information is available free of charge at https://pubs.acs.org/doi/10.1021/acsomega.5c02253.

EIS results for the analysis and a table with the value of each element in the circuit for every sample for every temperature (PDF)

AUTHOR INFORMATION

Corresponding Author

Yatir Sadia − *Faculty of Engineering Materials Engineering, Bar Ilan University, Ramat Gan 5290002, Israel; Material Engineering, Ben Gurion University of the Negev, Beer-Sheva 8410501, Israel; Department of Materials, Imperial College of London, London SW7 2AZ, U.K.;* orcid.org/0000-0001-9197-4481; Email: Yatir.Sadia@biu.ac.il

Authors

Gwilherm Kerherve − *Department of Materials, Imperial College of London, London SW7 2AZ, U.K.*

Stephen J. Skinner − *Department of Materials, Imperial College of London, London SW7 2AZ, U.K.;* orcid.org/0000-0001-5446-2647

Complete contact information is available at: https://pubs.acs.org/10.1021/acsomega.5c02253

Notes

The authors declare no competing financial interest.

ACKNOWLEDGMENTS

The authors would like to acknowledge Yair George's help with the sample preparation and hot pressing and Eng. Hagit Didi for SEM microscopy. They additionally thank Dr Arim Seong and Kehan Huang for their assistance with data collection. S.J.S. would like to acknowledge the Royal Academy of Engineering for the award of a Research Chair (RCSRF/2021-1243).

REFERENCES

(1) Nowroozi, M. A.; Mohammad, I.; Molaiyan, P.; Wissel, K.; Munnangi, A. R.; Clemens, O. Fluoride ion batteries−past, present, and future. *J. Mater. Chem. A* **2021**, *9* (10), 5980−6012.

(2) Miki, H.; Yamamoto, K.; Nakaki, H.; Yoshinari, T.; Nakanishi, K.; Nakanishi, S.; Iba, H.; Miyawaki, J.; Harada, Y.; Kuwabara, A.; Wang, Y.; et al. Double-layered perovskite oxyfluoride cathodes with high capacity involving O−O bond formation for fluoride-ion batteries. *J. Am. Chem. Soc.* **2024**, *146* (6), 3844−3853.

(3) Wang, Y.; Takami, T.; Li, Z.; Yamamoto, K.; Matsunaga, T.; Uchiyama, T.; Watanabe, T.; Miki, H.; Inoue, T.; Iba, H.; Mizutani, U.; et al. Oxyfluoride cathode for all-solid-state fluoride-ion batteries with small volume change using three-dimensional diffusion paths. *Chem. Mater.* **2022**, *34* (23), 10631−10638.

(4) Kim, S. W.; Pereira, N.; Chernova, N. A.; Omenya, F.; Gao, P.; Whittingham, M. S.; Amatucci, G. G.; Su, D.; Wang, F. Structure stabilization by mixed anions in oxyfluoride cathodes for high-energy lithium batteries. *ACS Nano* **2015**, *9* (10), 10076−10084.

(5) Reddy, M. V.; Madhavi, S.; Subba Rao, G. V.; Chowdari, B. V. R. Metal oxyfluorides $TiOF_2$ and NbO_2F as anodes for Li-ion batteries. *J. Power Sources* **2006**, *162* (2), 1312−1321.

(6) Zhang, L.; Dambournet, D.; Iadecola, A.; Batuk, D.; Borkiewicz, O. J.; Wiaderek, K. M.; Salager, E.; Shao, M.; Chen, G.; Tarascon, J. M. Origin of the high capacity manganese-based oxyfluoride electrodes for rechargeable batteries. *Chem. Mater.* **2018**, *30* (15), 5362−5372.

(7) Ando, M.; Enoki, M.; Nishiguchi, H.; Ishihara, T.; Takita, Y. Oxide ion conductivity and chemical stability of lanthanum fluorides doped with oxygen, La (Sr,Na)$F_{3-2X}O_X$. *Chem. Mater.* **2004**, *16* (21), 4109−4115.
(8) Tarasova, N. A.; Filinkova, Y. V.; Animitsa, I. E. Electric properties of oxyfluorides $Ba_2In_2O_{5-0.5x}F_x$ with brownmillerite structure. *Russ. J. Electrochem.* **2013**, *49*, 45−51.
(9) Momai, M.; Tamura, S.; Imanaka, N. Fluoride ion conducting behavior in nonstoichiometric lanthanum oxyfluoride. *Ceram. Int.* **2023**, *49* (1), 1502−1506.
(10) Motohashi, K.; Sanada, T.; Nakamura, T.; Kimura, Y.; Uchimoto, Y.; Amezawa, K. Revealing impacts of anion defect species on fluoride-ion conduction of Ruddlesden-popper oxyfluoride Ba_2ScO_3F. *Electrochemistry* **2022**, *90* (12), 127005.
(11) Abakumov, A. M.; Rozova, M. G.; Ardashnikova, E. I.; Antipov, E. V. High-temperature superconductors based on complex layered copper oxyfluorides. *Russ. Chem. Rev.* **2002**, *71* (5), 383−399.
(12) Kawashima, T.; Matsui, Y.; Takayama-Muromachi, E. New oxyfluoride superconductors $Sr_2Ca_{n-1}Cu_nO_{2n+\delta}F_{2\pm y}$ (n = 2; T_c= 99 K, n = 3; T_c = 111 K) prepared at high pressure. *Physica C* **1996**, *257* (3−4), 313−320.
(13) Mori, T.; Kajihara, K.; Kanamura, K.; Toda, Y.; Hiramatsu, H.; Hosono, H. Indium-based ultraviolet-transparent electroconductive oxyfluoride InOF: ambient-pressure synthesis and unique electronic properties in comparison with In_2O_3. *J. Am. Chem. Soc.* **2013**, *135* (35), 13080−13088.
(14) Atuchin, V. V.; Isaenko, L. I.; Kesler, V. G.; Kang, L.; Lin, Z.; Molokeev, M. S.; Yelisseyev, A. P.; Zhurkov, S. A. Structural, spectroscopic, and electronic properties of cubic G0-Rb_2KTiOF_5 oxyfluoride. *J. Phys. Chem. C* **2013**, *117* (14), 7269−7278.
(15) Takeiri, F.; Yamamoto, T.; Hayashi, N.; Hosokawa, S.; Arai, K.; Kikkawa, J.; Ikeda, K.; Honda, T.; Otomo, T.; Tassel, C.; Kimoto, K.; et al. $AgFeOF_2$: a fluorine-rich perovskite oxyfluoride. *Inorg. Chem.* **2018**, *57* (11), 6686−6691.
(16) Tsujimoto, Y.; Yamaura, K.; Takayama-Muromachi, E. Oxyfluoride chemistry of layered perovskite compounds. *Appl. Sci.* **2012**, *2* (1), 206−219.
(17) Slater, P. R.; Gover, R. K. B. Synthesis and structure of the new oxide fluoride $Sr_2TiO_3F_2$ from the low temperature fluorination of Sr_2TiO_4: an example of a staged fluorine substitution/insertion reaction. *J. Mater. Chem.* **2002**, *12* (2), 291−294.
(18) Wissel, K.; Vogel, T.; Dasgupta, S.; Fortes, A. D.; Slater, P. R.; Clemens, O. Topochemical fluorination of n = 2 Ruddlesden−Popper type $Sr_3Ti_2O_7$ to $Sr_3Ti_2O_5F_4$ and its reductive defluorination. *Inorg. Chem.* **2020**, *59* (2), 1153−1163.
(19) Yu, J.; Xu, X. Fluorination over Cr doped layered perovskite Sr_2TiO_4 for efficient photocatalytic hydrogen production under visible light illumination. *J. Energy Chem.* **2020**, *51*, 30−38.
(20) Khenata, R.; Daoudi, B.; Sahnoun, M.; Baltache, H.; Rérat, M.; Reshak, A. H.; Bouhafs, B.; Abid, H.; Driz, M. Structural, electronic and optical properties of fluorite-type compounds. *Eur. Phys. J. B* **2005**, *47*, 63−70.
(21) Voronin, B. M.; Volkov, S. V. Ionic conductivity of fluorite type crystals CaF_2, SrF_2, BaF_2, and $SrCl_2$ at high temperatures. *J. Phys. Chem. Solids* **2001**, *62* (7), 1349−1358.
(22) Druon, F.; Ricaud, S.; Papadopoulos, D. N.; Pellegrina, A.; Camy, P.; Doualan, J. L.; Moncorgé, R.; Courjaud, A.; Mottay, E.; Georges, P. On Yb: CaF_2 and Yb: SrF_2: review of spectroscopic and thermal properties and their impact on femtosecond and high power laser performance. *Opt. Mater. Express* **2011**, *1* (3), 489−502.
(23) Dorenbos, P.; Den Hartog, H. W.; Kruizinga, R.; Vrind, S. Hopping ionic conductivity in Ce-doped SrF_2. II. Results obtained from impedance measurements. *Phys. Rev. B* **1987**, *35* (11), 5774.
(24) Bollmann, W.; Görlich, P.; Hauk, W.; Mothes, H. Ionic conduction of pure and doped CaF_2 and SrF_2 crystals. *Phys. Status Solidi A* **1970**, *2* (1), 157−170.
(25) Meuldijk, J.; Den Hartog, H. W. Ionic thermocurrents and ionic conductivity of solid solutions of SrF_2 and YbF_3. *Phys. Rev. B* **1983**, *27* (10), 6376.
(26) Sorokin, N. I.; Sobolev, B. P. Anionic high-temperature conduction in single crystals of nonstoichiometric phases $R_{1-y}M_yF_{3-y}$ (R = La-Lu, M = Ca, Sr, Ba) with the tysonite (LaF_3) structure. *Russ. J. Electrochem.* **2007**, *43*, 398−409.
(27) Dieudonné, B.; Chable, J.; Body, M.; Legein, C.; Durand, E.; Mauvy, F.; Fourcade, S.; Leblanc, M.; Maisonneuve, V.; Demourgues, A. The key role of the composition and structural features in fluoride ion conductivity in tysonite $Ce_{1-x}Sr_xF_{3-x}$ solid solutions. *Dalton Trans.* **2017**, *46* (11), 3761−3769.
(28) Dieudonné, B.; Chable, J.; Mauvy, F.; Fourcade, S.; Durand, E.; Lebraud, E.; Leblanc, M.; Legein, C.; Body, M.; Maisonneuve, V.; Demourgues, A. Exploring the $Sm_{1-x}Ca_xF_{3-x}$ tysonite solid solution as a solid-state electrolyte: relationships between structural features and F^- ionic conductivity. *J. Phys. Chem. C* **2015**, *119* (45), 25170−25179.
(29) Shafer, M. W.; Chandrashekhar, G. V.; Figat, R. A. New fluoride ion conductor, $K_xBi_{1-x}F_{3-2x}$ ($.02 \leq x \leq .12$), with the tysonite structure. *Solid State Ionics* **1981**, *5*, 633−635.
(30) Rongeat, C.; Reddy, M. A.; Witter, R.; Fichtner, M. Nanostructured fluorite-type fluorides as electrolytes for fluoride ion batteries. *J. Phys. Chem. C* **2013**, *117* (10), 4943−4950.
(31) Mori, K.; Mineshige, A.; Saito, T.; Sugiura, M.; Ishikawa, Y.; Fujisaki, F.; Namba, K.; Kamiyama, T.; Otomo, T.; Abe, T.; Fukunaga, T. Experimental visualization of interstitialcy diffusion pathways in fast-fluoride-ion-conducting solid electrolyte $Ba_{0.6}La_{0.4}F_{2.4}$. *ACS Appl. Energy Mater.* **2020**, *3* (3), 2873−2880.
(32) Heise, M.; Scholz, G.; Düvel, A.; Heitjans, P.; Kemnitz, E. Mechanochemical synthesis, structure, and properties of solid solutions of alkaline earth metal fluorides: $M^a_{1-x}M^b_xF_2$ (M: Ca, Sr, Ba). *Solid State Sci.* **2016**, *60*, 65−74.
(33) Wang, J.; Hao, J.; Duan, C.; Wang, X.; Wang, K.; Ma, C. A fluoride-ion-conducting solid electrolyte with both high conductivity and excellent electrochemical stability. *Small* **2022**, *18* (5), 2104508.
(34) Wang, J.; Ma, C. Superior room-temperature cycling stability of fluoride-ion batteries enabled by solid electrolytes synthesized by the solid-state reaction. *Sci. China Mater.* **2022**, *65* (11), 3025−3032.
(35) Yamane, Y.; Yamada, K.; Inoue, K. Mechanochemical synthesis and order−disorder phase transition in fluoride ion conductor $RbPbF_3$. *Solid State Ionics* **2008**, *179* (17−18), 605−610.
(36) Kavun, V. Y.; Uvarov, N. F.; Goncharuk, V. K.; Merkulov, E. B.; Ulikhin, A. S.; Telin, I. A.; Kharchenko, V. I. Ion mobility and transport properties of fluorite-type solid solutions in the PbF_2−BiF_3−MF systems (M = Rb, Cs) according to NMR and conductivity data. *Solid State Ionics* **2014**, *257*, 17−22.
(37) *Inorganic Solid Fluorides: Chemistry and Physics*; Hagenmuller, P., Ed.; Elsevier, 2012.
(38) Sorokin, N. I.; Fedorov, P. P.; Zakalyukin, R. M.; Sobolev, B. P.; Boltalin, A. I.; Val'kovskij, M. D. Electric conductivity of fluoride glasses on the base of PbF_2 and InF_3 Ehlektroprovodnost'ftoridnykh stekol na osnove PbF_2 InF_3. *Neorg. Mater.* **1999**, *35*, 88−89.
(39) Pohorenko, Y.; Pshenychnyi, R. M.; Pavlenko, T.; Omelchuk, A.; Trachevskyi, V. Fluoride ion Conductivity of Solid Solutions $K_xPb_{0.86-x}Sn_{1.14}F_{4-x}$. *J. Serb. Chem. Soc.* **2021**, *86* (9), 845−857.
(40) Uno, M.; Onitsuka, M.; Ito, Y.; Yoshikado, S. Synthesis and evaluation of $Pb_{1-x}Sn_xF_2$ by mechanical milling. *Solid State Ionics* **2005**, *176* (31−34), 2493−2498.
(41) Kanno, R.; Nakamura, S.; Kawamoto, Y. Ionic conductivity of tetragonal $PbSnF_4$ substituted by aliovalent cations Zr^{4+}, Al^{3+}, Ga^{3+}, In^{3+} and Na^+. *Solid State Ionics* **1992**, *51* (1−2), 53−59.
(42) Pogorenko, Y. V.; Pshenychnyi, R. M.; Omelchuk, A. O.; Trachevskyi, V. V. Conductivity of aliovalent substitution solid solutions $Pb_{1-x}R_xSnF_{4+x}$ (R = Y, La, Ce, Nd, Sm, Gd) with β-$PbSnF_4$ structure. *Solid State Ionics* **2019**, *338*, 80−86.
(43) Liu, L.; Yang, L.; Liu, M.; Li, X.; Shao, D.; Luo, K.; Wang, X.; Luo, Z. SnF_2-based fluoride ion electrolytes $MSnF_4$ (M = Ba, Pb) for the application of room-temperature solid-state fluoride ion batteries. *J. Alloys Compd.* **2020**, *819*, 152983.
(44) Zhang, J.; Zhou, P.; Liu, J.; Yu, J. New understanding of the difference of photocatalytic activity among anatase, rutile and brookite TiO_2. *Phys. Chem. Chem. Phys.* **2014**, *16* (38), 20382−20386.

https://doi.org/10.1021/acsomega.5c02253
ACS Omega 2025, 10, 19214−19223

(45) Nowotny, J.; Radecka, M.; Rekas, M.; Sugihara, S.; Vance, E. R.; Weppner, W. Electronic and ionic conductivity of TiO_2 single crystal within the n−p transition range. *Ceram. Int.* **1998**, *24* (8), 571−577.
(46) Tang, J.; Wang, W.; Zhao, G. L.; Li, Q. Colossal positive Seebeck coefficient and low thermal conductivity in reduced TiO_2. *J. Phys.: Condens. Matter* **2009**, *21* (20), 205703.
(47) Nowotny, M. K.; Bak, T.; Nowotny, J. Electrical properties and defect chemistry of TiO_2 single crystal. I. Electrical conductivity. *J. Phys. Chem. B* **2006**, *110* (33), 16270−16282.
(48) Tannhauser, D. S. Experimental evidence from conductivity measurements for interstitial titanium in reduced TiO_2. *Solid State Commun.* **1963**, *1* (7), 223−225.
(49) Sheppard, L. R.; Nowotny, M. K.; Bak, T.; Nowotny, J. Effect of cooling on electrical conductivity of TiO_2. *Phys. Status Solidi B* **2008**, *245* (9), 1816−1827.
(50) Wang, J.; Cao, F.; Bian, Z.; Leung, M. K.; Li, H. Ultrafine single-crystal $TiOF_2$ nanocubes with mesoporous structure, high activity and durability in visible light driven photocatalysis. *Nanoscale* **2014**, *6* (2), 897−902.
(51) Saputera, W. H.; Yuniar, G.; Sasongko, D. Light-driven methane conversion: unveiling methanol using a $TiO_2/TiOF_2$ photocatalyst. *RSC Adv.* **2024**, *14* (13), 8740−8751.
(52) Hou, C.; Liu, W. One-step synthesis of OH-$TiO_2/TiOF_2$ nanohybrids and their enhanced solar light photocatalytic performance. *R. Soc. Open Sci.* **2018**, *5* (6), 172005.
(53) Hou, C.; Liu, H.; Li, Y. The preparation of three-dimensional flower-like $TiO_2/TiOF_2$ photocatalyst and its efficient degradation of tetracycline hydrochloride. *RSC Adv.* **2021**, *11* (25), 14957−14969.
(54) Reddy, M. V.; Madhavi, S.; Subba Rao, G. V.; Chowdari, B. V. R. Metal oxyfluorides $TiOF_2$ and NbO_2F as anodes for Li-ion batteries. *J. Power Sources* **2006**, *162* (2), 1312−1321.
(55) Li, B.; Wang, D.; Wang, Y.; Zhu, B.; Gao, Z.; Hao, Q.; Wang, Y.; Tang, K. One-step synthesis of hexagonal $TiOF_2$ as high rate electrode material for lithium-ion batteries: research on Li intercalation/de-intercalation mechanism. *Electrochim. Acta* **2015**, *180*, 894−901.
(56) Zeng, Y.; Zhang, W.; Xu, C.; Xiao, N.; Huang, Y.; YW Yu, D.; Hng, H. H.; Yan, Q. One-step solvothermal synthesis of single-crystalline $TiOF_2$ nanotubes with high lithium-ion battery performance. *Chem.—Eur. J.* **2012**, *18* (13), 4026−4030.
(57) Astrova, E. V.; Parfeneva, A. V.; Li, G. V.; Ulin, V. P.; Yagovkina, M. A.; Nashchekin, A. V.; Beregulin, E. V.; Rumyantsev, A. M. Anodes for Li-ion batteries based on titanium fluorides. *Energy Storage* **2024**, *6* (2), No. e594.
(58) Jung, M. J.; Kim, Y.; Lee, Y. S. Enhancement of the electrochemical capacitance of $TiOF_2$ obtained via control of the crystal structure. *J. Ind. Eng. Chem.* **2017**, *47*, 187−193.
(59) Tamgadge, R. M.; Shukla, A. Fluorine-doped anatase for improved supercapacitor electrode. *Electrochim. Acta* **2018**, *289*, 342−353.
(60) Shian, S.; Sandhage, K. H. Hexagonal and cubic $TiOF_2$. *J. Appl. Crystallogr.* **2010**, *43* (4), 757−761.
(61) Lv, K.; Yu, J.; Cui, L.; Chen, S.; Li, M. Preparation of thermally stable anatase TiO_2 photocatalyst from $TiOF_2$ precursor and its photocatalytic activity. *J. Alloys Compd.* **2011**, *509* (13), 4557−4562.
(62) Kowalkińska, M.; Dudziak, S.; Karczewski, J.; Ryl, J.; Trykowski, G.; Zielińska-Jurek, A. Facet effect of TiO_2 nanostructures from $TiOF_2$ and their photocatalytic activity. *Chem. Eng. J.* **2021**, *404*, 126493.
(63) Shi, X. L.; Wu, H.; Liu, Q.; Zhou, W.; Lu, S.; Shao, Z.; Dargusch, M.; Chen, Z. G. $SrTiO_3$-based thermoelectrics: progress and challenges. *Nano Energy* **2020**, *78*, 105195.
(64) Muta, H.; Kurosaki, K.; Yamanaka, S. Thermoelectric properties of rare earth doped $SrTiO_3$. *J. Alloys Compd.* **2003**, *350* (1−2), 292−295.
(65) Sun, J.; Singh, D. J. Thermoelectric properties of n-type $SrTiO_3$. *APL Mater.* **2016**, *4* (10), 104803.
(66) Chen, G.; Zhu, B.; Deng, H.; Luo, Y.; Sun, W.; Liu, H.; Zhang, W.; Wang, X.; Qian, Y.; Hu, X.; Geng, S.; et al. Advanced fuel cell based on perovskite La−$SrTiO_3$ semiconductor as the electrolyte with superoxide-ion conduction. *ACS Appl. Mater. Interfaces* **2018**, *10* (39), 33179−33186.
(67) Torabi, A.; Etsell, T. H. Electrochemical behavior of solid oxide fuel cell anodes based on infiltration of Y-doped $SrTiO_3$. *J. Power Sources* **2013**, *225*, 51−59.
(68) Shah, M. Y.; Rauf, S.; Zhu, B.; Mushtaq, N.; Yousaf, M.; Lund, P. D.; Xia, C.; Asghar, M. I. Semiconductor Nb-doped $SrTiO_{3-\delta}$ perovskite electrolyte for a ceramic fuel cell. *ACS Appl. Energy Mater.* **2021**, *4* (1), 365−375.
(69) Li, Y.; Niu, S.; Wang, J.; Zhou, W.; Wang, Y.; Han, K.; Lu, C. Mesoporous $SrTiO_3$ perovskite as a heterogeneous catalyst for biodiesel production: experimental and DFT studies. *Renewable Energy* **2022**, *184*, 164−175.
(70) Li, Y.; Niu, S.; Hao, Y.; Zhou, W.; Wang, J.; Liu, J. Role of oxygen vacancy on activity of Fe-doped $SrTiO_3$ perovskite bifunctional catalysts for biodiesel production. *Renewable Energy* **2022**, *199*, 1258−1271.
(71) Ghani, N.; Iqbal, J.; Sadaf, S.; Bhatti, H. N.; Asgher, M. A facile approach for the synthesis of $SrTiO_3$/g-C_3N_4 photo-catalyst and its efficacy in biodiesel production. *ChemistrySelect* **2021**, *6* (43), 12082−12093.
(72) Lee, C. H.; Podraza, N. J.; Zhu, Y.; Berger, R. F.; Shen, S.; Sestak, M.; Collins, R. W.; Kourkoutis, L. F.; Mundy, J. A.; Wang, H.; Mao, Q.; et al. Effect of reduced dimensionality on the optical band gap of $SrTiO_3$. *Appl. Phys. Lett.* **2013**, *102* (12), 122901.
(73) Toby, B. H.; Von Dreele, R. B. GSAS-II: the genesis of a modern open-source all purpose crystallography software package. *J. Appl. Crystallogr.* **2013**, *46* (2), 544−549.
(74) Wyckoff, R. New York rocksalt structure. In *Crystal Structures*; Interscience Publishers: New York, 1963; Vol. *1*, pp 85−237.
(75) Seki, H.; Ishizawa, N.; Mizutani, N.; Kato, M. High-temperature structures of the rutile-type oxides, TiO_2 and SnO_2. *J. Ceram. Soc. Jpn.* **1984**, *92* (1064), 219−223.
(76) Natu, V.; Benchakar, M.; Canaff, C.; Habrioux, A.; Celerier, S.; Barsoum, M. W. A critical analysis of the X-ray photoelectron spectra of $Ti_3C_2T_z$ MXenes. *Matter* **2021**, *4* (4), 1224−1251.
(77) Guan, S.; Fan, Q.; Shen, Z.; Zhao, Y.; Sun, Y.; Shi, Z. Heterojunction TiO_2@$TiOF_2$ nanosheets as superior anode materials for sodium-ion batteries. *J. Mater. Chem. A* **2021**, *9* (9), 5720−5729.
(78) Klimov, V. D.; Vashman, A. A.; Pronin, I. S. Study of atomic titanium interaction with PF_3 matrix at 77-K-cryochemical synthesis of TiF_2. PF_3 monotriphosphinetitanium (II) fluoride new compounds. *Zh. Obshch. Khim.* **1991**, *61* (10), 2166−2174.
(79) Subash, B.; Krishnakumar, B.; Velmurugan, R.; Swaminathan, M. Photodegradation of an azo dye with reusable SrF_2−TiO_2 under UV light and influence of operational parameters. *Sep. Purif. Technol.* **2012**, *101*, 98−106.
(80) Singh, R.; Thakur, R. P. S.; Katz, A.; Nelson, A. J.; Gebhard, S. C.; Swartzlander, A. B. Relationship between thermal stress and structural properties of SrF_2 films on (100) InP. *Appl. Phys. Lett.* **1990**, *57* (12), 1239−1241.
(81) Chambers, S. A.; Droubay, T. C.; Capan, C.; Sun, G. Y. Unintentional F doping of $SrTiO_3$ (001) etched in HF acid-structure and electronic properties. *Surf. Sci.* **2012**, *606* (3−4), 554−558.
(82) Rongeat, C.; Reddy, M. A.; Witter, R.; Fichtner, M. Nanostructured fluorite-type fluorides as electrolytes for fluoride ion batteries. *J. Phys. Chem. C* **2013**, *117* (10), 4943−4950.
(83) Huggins, R. A. Simple method to determine electronic and ionic components of the conductivity in mixed conductors a review. *Ionics* **2002**, *8*, 300−313.
(84) Jonscher, A. K. Analysis of the alternating current properties of ionic conductors. *J. Mater. Sci.* **1978**, *13*, 553−562.
(85) Gavarri, J. R.; Tortet, L.; Musso, J. Transport properties and percolation in two-phase composites. *Solid State Ionics* **1999**, *117* (1−2), 75−85.

https://doi.org/10.1021/acsomega.5c02253
ACS Omega 2025, 10, 19214−19223

(86) Synodis, M. J.; Porter, C. L.; Vo, N. M.; Reszka, A. J.; Gross, M. D.; Snyder, R. C. A model to predict percolation threshold and effective conductivity of infiltrated electrodes for solid oxide fuel cells. *J. Electrochem. Soc.* **2013**, *160* (11), F1216.
(87) Li, C.; Gu, L.; Guo, X.; Samuelis, D.; Tang, K.; Maier, J. Charge carrier accumulation in lithium fluoride thin films due to Li-ion absorption by titania (100) subsurface. *Nano Lett.* **2012**, *12* (3), 1241−1246.
(88) Sorokin, N. I.; Karimov, D. N.; Sulyanova, E. A.; Zhmurova, Z. I.; Sobolev, B. P. Nanostructured crystals of fluorite phases $Sr_{1-x}R_xF_{2+x}$ (R are rare earth elements) and their ordering: 5. A study of the ionic conductivity of as-grown $Sr_{1-x}R_xF_{2+x}$ crystals. *Crystallogr. Rep.* **2010**, *55*, 662−667.
(89) Ahmad, M. M.; Yamada, K.; Okuda, T. Ionic conduction and relaxation in KSn_2F_5 fluoride ion conductor. *Physica B* **2003**, *339* (2−3), 94−100.

https://doi.org/10.1021/acsomega.5c02253
ACS Omega 2025, 10, 19214−19223